

***In Silico Activation of Dinitrogen with a Light Atom Molecule***

Stefan Mebs,<sup>1\*</sup> Jens Beckmann<sup>2</sup>

<sup>1</sup> *Institut für Experimentalphysik, Freie Universität Berlin, Arnimallee 14, 14195 Berlin, Germany*

<sup>2</sup> *Institut für Anorganische Chemie und Kristallographie, Universität Bremen, Leobener Straße 7, 28359 Bremen, Germany*

**Supporting information**

## 1-spacer approach

The conceptual design should include frustrated Lewis acid-base pairs (FLPs), with a flexible distance towards each other and the use of bulky substituents at the central LA/LB atoms to prevent the formation of quenched “dead-end” states with a strong LA–LB connection. Single-spacer approaches can contain a FLP, which indeed is sterically blocked, but the required structural dynamics are only possible, if the spacer group itself is flexible. Ideally, the relaxed spacer molecule is flat, but being bend by the ongoing LA–LB bonding, thus releasing additional relaxation energy *via* N<sub>2</sub>-adduct formation. Moreover, the spacer group itself needs to carry a second LA atom, which was found to be essential for energy efficient N<sub>2</sub>-fixation. A spacer group with the desired properties was found in the 10-hydro-10-boro-9,9-dimethyl-9-silaanthracene ligand system (Figure S1, left side), which both carries a LA atom (B) and is flexible towards bending, see below. However, extended variations of substituents both at the LA or LB atom as well as on the B atom of the spacer group uncovered the essential role of another (very) bulky substituent at the B atom to prevent premature relaxation of the spacer group *via* forming a quenched state. As a result, only the structure presented in Figures S1 (right side) and S2 proved to be capable of N<sub>2</sub>-activation. Hydride abstraction from the neutral ligand (-Mes<sub>2</sub>SiH, not shown) to reach the active state is feasible ( $-19.3\text{ kJ mol}^{-1}$ ) using the Ph<sub>3</sub>C<sup>+</sup> ion as hydride abstraction reagent. Although the energy gain of 103.8 kJ mol<sup>-1</sup> for N<sub>2</sub>-adduct formation is high, and the fact that the presence of a dead-end-state is unlikely (the state presented here as “dead-end”-state is 17.6 kJ mol<sup>-1</sup> higher in energy), the high complexity of the structural design makes a chemical synthesis in the laboratory also rather unlikely. Nevertheless, the structure may serve as blueprint for advanced structural design in the laboratory.

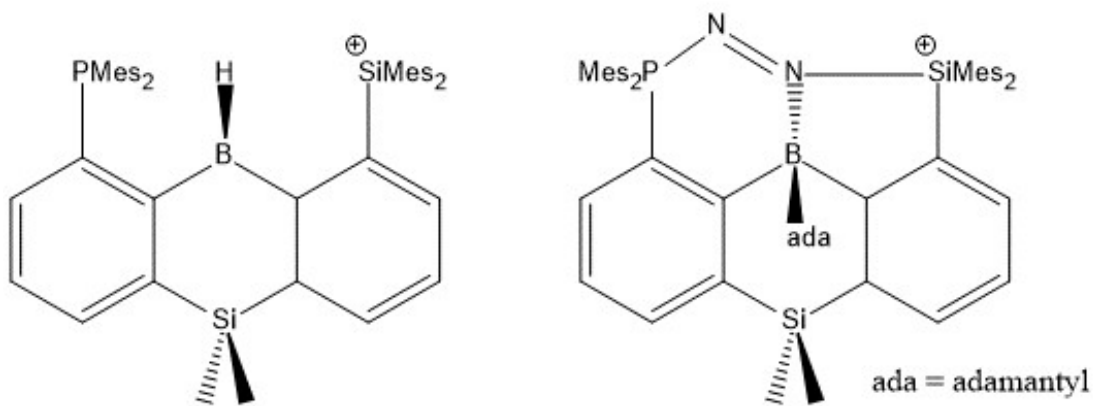


**Figure S1.** Structural design of a hypothetical compound being capable of N<sub>2</sub>-activation within the 1-spacer approach.

**Table S1.** Relevant geometric parameters for the 1-spacer approach (Å, °)

state	P-Si	P-B	Si-B	N-N	N-N(gas)	Δ
neutral	4.261	3.007	3.356			
active	4.329	2.939	3.464			
dead-end	4.931	3.374	3.428			
N <sub>2</sub> -adduct	4.372	3.128	2.883	1.240	1.091	0.150
state	P-N(1)	Si-N(2)	B-N(2)	P-N-N	Si-N-N	B-N-N
N <sub>2</sub> -adduct	1.753	1.896	1.567	119.6	117.2	129.9

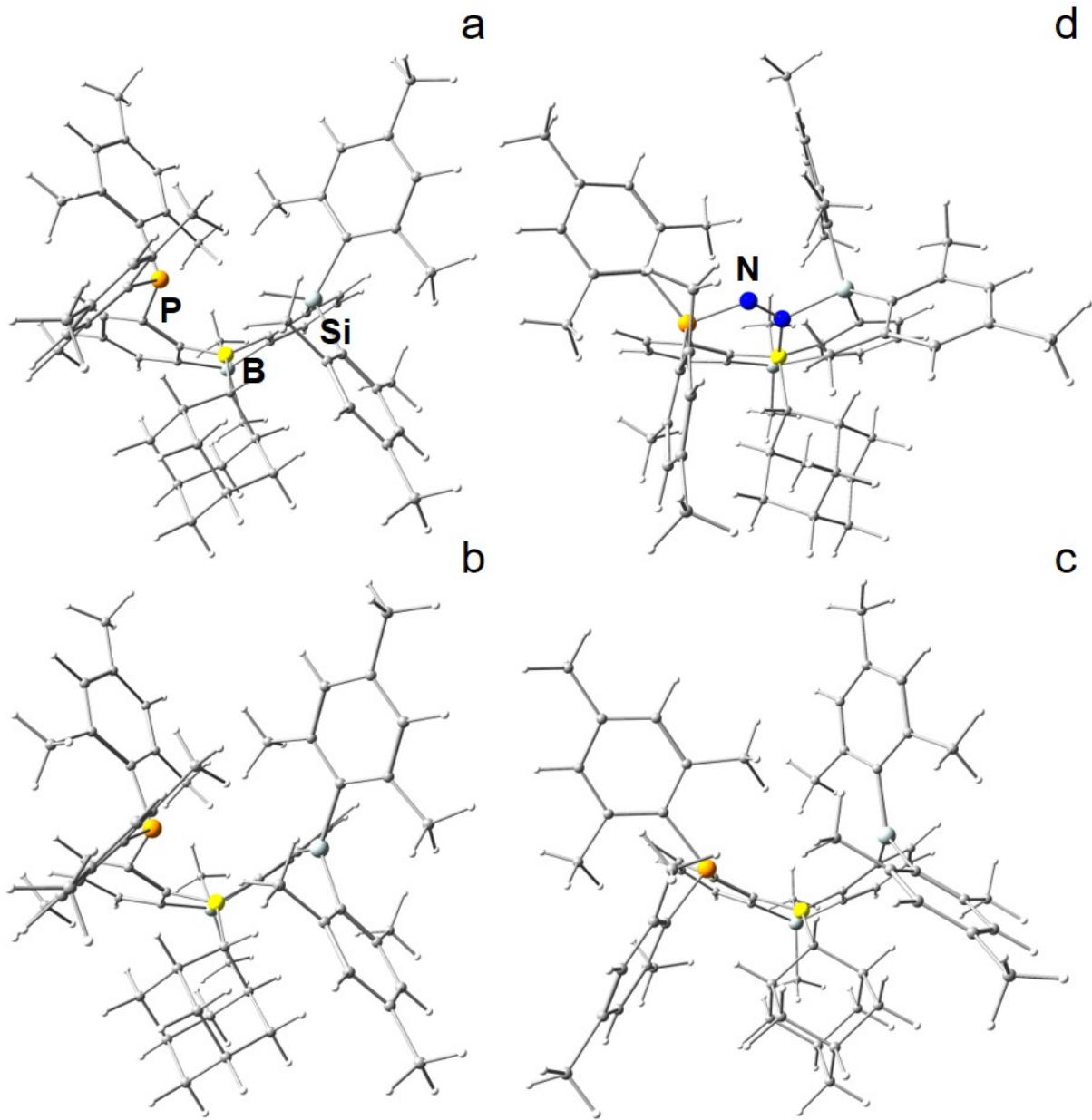


**Figure S2.** 1-spacer approach; DFT-relaxed geometries on the b3pw91-D3/6-311+G(2df,p) level of theory. (a) neutral ligand system. (b) active state (c) “dead-end” state. (d) N<sub>2</sub>-adduct.

## 2-spacer approach

Using two spacer groups, which are connected by a central LA or LB atom opens a large parameter-space in structural design, includes by definition more than one LA and/or LB, and makes the structures very flexible. However, especially the high degree of flexibility turned out to be disadvantageous as for almost each “active” state, which might be capable of energy efficient N<sub>2</sub>-activation, a dead-end state could be constructed with a strong LA–LB bond. Moreover, chemical synthesis might even be more complex, not to say, impossible by known routes. Accordingly, this approach was not followed further on, and the ligand system shown in Figure S3 and S4 is the only one for which the dead-end state was higher in energy than the active state (by 29.7 kJ mol<sup>-1</sup>), and for which N<sub>2</sub>-adduct formation was *almost* energy efficient (+10.8 kJ mol<sup>-1</sup> for N<sub>2</sub>(v1), Fig. S4c; +5.8 kJ mol<sup>-1</sup> for N<sub>2</sub>(v2), Fig. S4d). Although, the ligand system is not really capable of energy efficient N<sub>2</sub>-activation, it is for CO-activation (-27.1 kJ mol<sup>-1</sup>) and CO<sub>2</sub>-activation (-135.8 kJ mol<sup>-1</sup>). Hydride abstraction from the neutral ligand (-Si(C<sub>6</sub>F<sub>5</sub>)<sub>2</sub>H, not shown) to reach the active state might be feasible (+6.3 kJ mol<sup>-1</sup>) using the Ph<sub>3</sub>C<sup>+</sup> ion as hydride abstraction reagent.

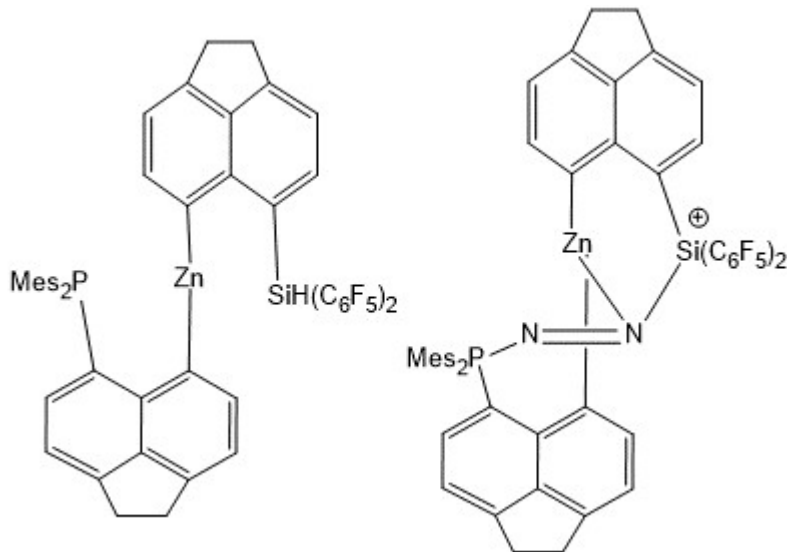


**Figure S3.** Structural design of a hypothetical compound being capable of N<sub>2</sub>-activation within the 2-spacer approach.

**Table S2.** Relevant geometric parameters for the 2-spacer approach (Å, °)

state	P-Si	P-Zn	Si-Zn	N-N	N-N(gas)	Δ(N-N)
active	2.561	3.261	3.209			
dead-end	4.744	2.502	2.608			
N <sub>2</sub> (v1)-add.	4.352	3.265	3.286	1.218	1.091	0.127
N <sub>2</sub> (v2)-add.	4.335	3.339	3.175	1.221	1.091	0.131
state	P-Si	P-Zn	Si-Zn	C-O	C-O <sub>1,2</sub> (gas)	Δ(C-O)
CO-add.	4.349	3.441	3.267	1.284	1.125	0.160
CO <sub>2</sub> -add.	4.398	3.530	3.254	1.314/1.190	1.158	0.156
state	P-N(1)	Si-N(2)	Zn-N	P-N-N	Si-N-N	Zn-N-N
N <sub>2</sub> (v1)-add.	1.790	1.844	2.276	128.3	113.4	124.6
N <sub>2</sub> (v2)-add.	1.818	1.809	2.225	113.5	127.1	128.7
state	P-C	Si-O	Zn-O	P-C-O	Si-O-C	Zn-O-C
CO-add.	1.925	1.735	2.431	109.0	130.2	127.8
CO <sub>2</sub> -add.	1.911	1.723	2.422	111.8	132.5	121.3

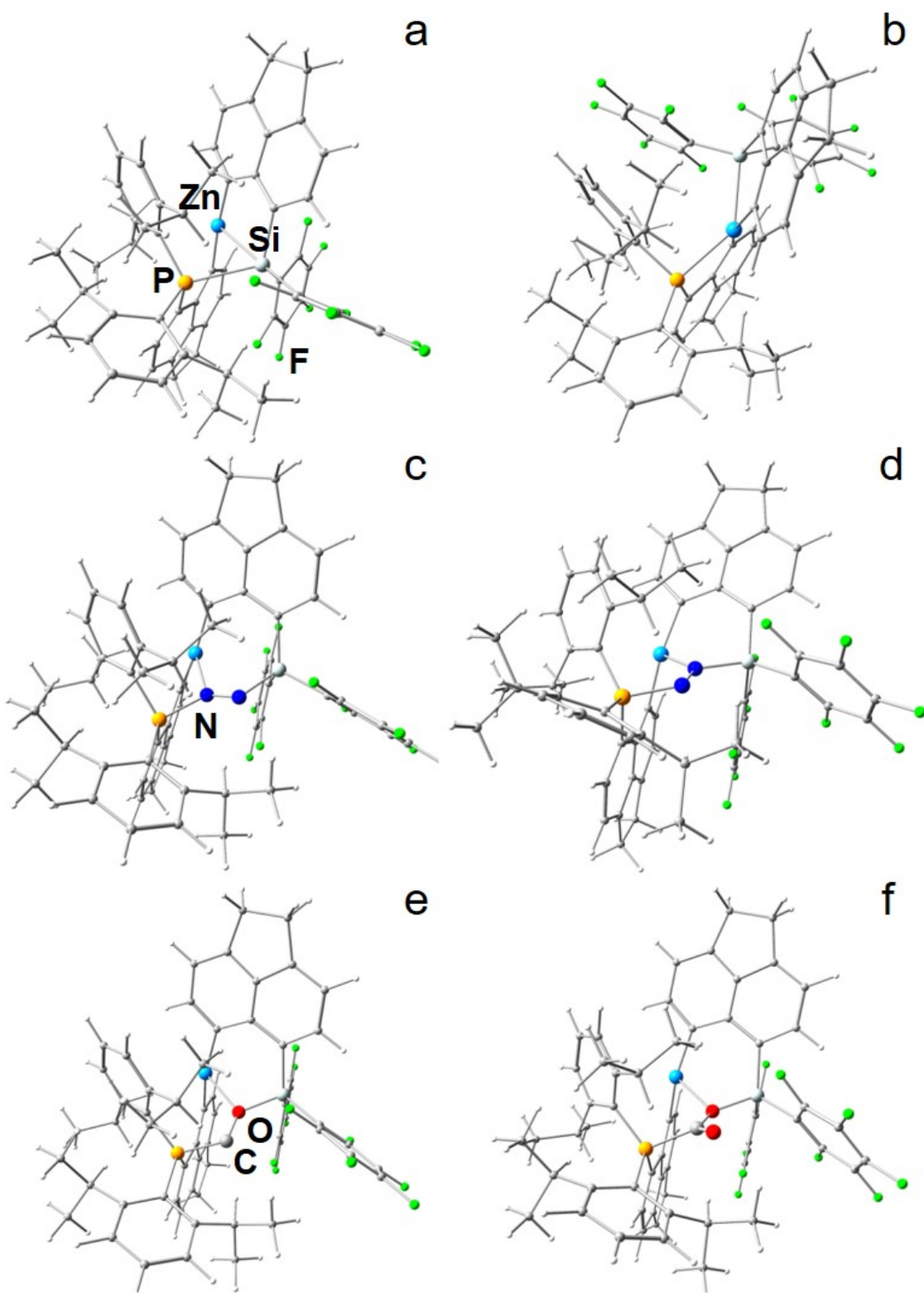


**Figure S4.** 2-spacer approach; DFT-relaxed geometries on the b3pw91-D3/6-311+G(2df,p) level of theory. (a) active state. (b) dead-end state. (c) and (d) N<sub>2</sub>-adducts. (e) CO-adduct. (f) CO<sub>2</sub>-adduct.

### 3-spacer approach

Since the addition of a third spacer likely would make chemical synthesis even more complex, structures based on that approach must be as simple as possible, i.e. containing only one type of LA-fragment (e.g.  $-\text{Ph}_2\text{Si}^+$ ) and an accessible second LB-fragment (e.g.  $\text{PPh}_2$ ), as shown in the main text. Seemingly, the formation of an energetically lower-lying dead-end state is possible by introduction of very bulky substituents, e.g. the use of  $-\text{Mes}_2\text{Si}^+$  instead of  $-\text{Ph}_2\text{Si}^+$  (see Figure S5), but this turned out to be a misconception, since every change of parameters (spacer group, LA/LB atom, substituents) can give rise to the formation of new unexpected structural motifs, many of which might be disadvantageous for  $\text{N}_2$ -activation.

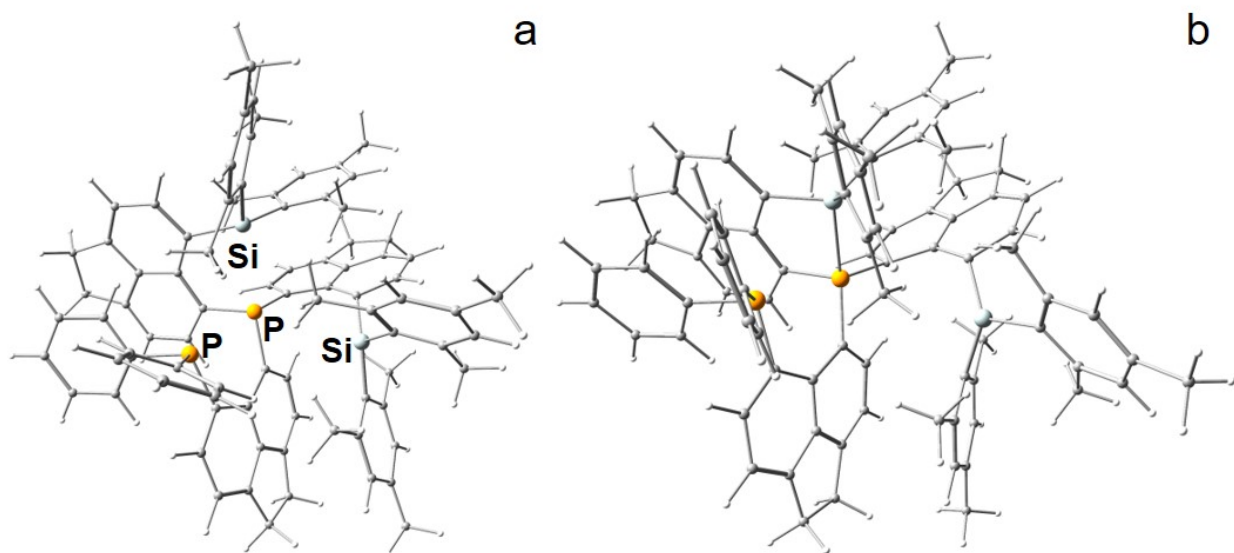


**Figure S5.** 3-spacer approach including mesityl substituents at the LA; DFT-relaxed geometries at the b3pw91-D3/6-31+G\* level of theory. (a) active state. (b) dead-end state. The dead-end state is still 42.4 kJ mol<sup>-1</sup> lower in energy than the active state.

**Table S3.** Relevant geometric parameters for the 3-spacer approach ( $\text{\AA}$ ,  $^\circ$ ): Mes-variant

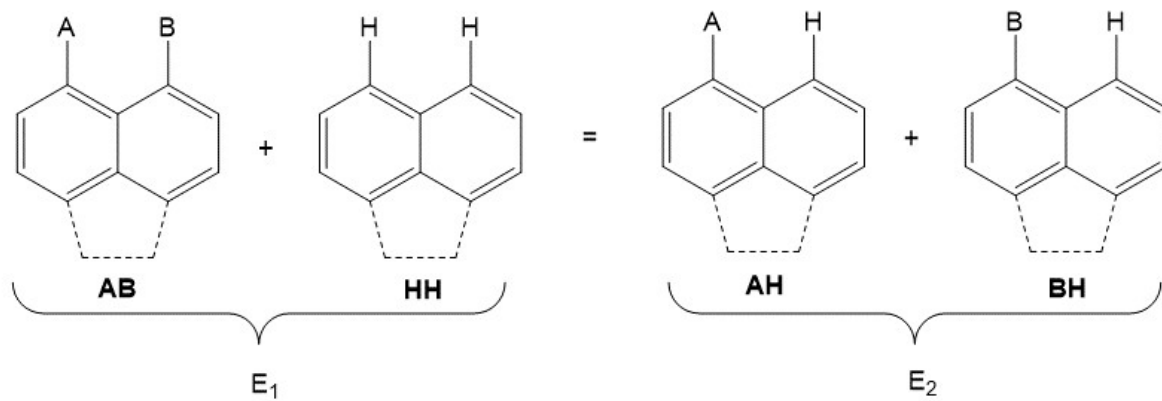
state	P(1)-P(2)	P(1)-Si(1)	P(1)-Si(2)	P(2)-Si(1)	P(2)-Si(2)	Si(1)-Si(2)
active	3.145	2.873	3.583	4.318	5.207	5.080
dead-end	3.144	2.379	4.083	3.381	5.999	5.027

**Table S4.** Absolute and relative molecular energies for the 3-spacer approach

model	details	E	$\Delta E$ [a.u.]	$\Delta E$ [kJ mol <sup>-1</sup> ]	ligand +small	details	$\Delta E$ [a.u.]	details	$\Delta E$ [kJ mol <sup>-1</sup> ]
N <sub>2</sub>		-109.5178							
$\frac{1}{2}$ B <sub>2</sub> H <sub>6</sub>		-26.6433							
BH <sub>4</sub> <sup>(-)</sup>		-27.3524	-0.7091	-1861.8					
CPh <sub>3</sub> <sup>(+)</sup>		-732.8735							
CPh <sub>3</sub> H		-733.6787	-0.8052	-2114.0					
Tf <sup>(-)</sup>		-961.6323							
TfH		-962.0547	-0.4224	-1109.0					
1a	endo-endo	-4039.2632	0.0040	10.4					
1b	exo-exo	-4039.2478	0.0194	50.9					
1c = <b>1</b>	exo-endo	-4039.2671			-4772.1407	1+CPh <sub>3</sub> <sup>(+)</sup>			
<b>2</b>		-4038.5504			-4772.2291	2+CPh <sub>3</sub> H	-0.0884	(2+CPh <sub>3</sub> H) - (1+CPh <sub>3</sub> <sup>(+)</sup> )	-232.1
<b>3a</b>		-4037.7462			-4771.4249	3a+CPh <sub>3</sub> H	-0.0010	(3a+CPh <sub>3</sub> H) - (2+CPh <sub>3</sub> <sup>(+)</sup> )	-2.6
3b		-4037.7225	0.0237	62.2	-4147.2640	3a+N <sub>2</sub>	-0.0616	4b-(3a+N <sub>2</sub> )	-161.6
4a		-4147.3118	0.0137	36.1					
<b>4b</b>		-4147.3255			-4174.6779	4b+BH <sub>4</sub> <sup>(-)</sup>			
4c		-4147.2875	0.0380	99.8					
<b>5a</b>	N(1)-endo	-4148.1271			-4174.7703	5+ $\frac{1}{2}$ B <sub>2</sub> H <sub>6</sub>	-0.0924	(5+ $\frac{1}{2}$ B <sub>2</sub> H <sub>6</sub> ) - (4+BH <sub>4</sub> <sup>(-)</sup> )	-242.6
5b	N(2)-exo	-4148.1081	0.0190	49.8	-4174.7514		-0.0734		-192.7
5c	Si(1)-endo	-4148.0438	0.0833	218.6	-4174.6871		-0.0091		-24.0
5d	Si(1)-exo	-4148.0327	0.0943	247.7	-4174.6760		0.0019		5.1
5e	Si(2)-endo	-4148.0259	0.1011	265.5	-4174.6692		0.0087		22.9
5f	Si(2)-exo	-4148.0139	0.1132	297.1	-4174.6572		0.0208		54.5
6a	H <sup>+</sup> @N(1)	-4148.5654			-5110.1818	5+TfH			
6b	H <sup>+</sup> @N(2)	-4148.5506	0.0148	38.8	-5110.1977	6+Tf <sup>(+)</sup>	-0.0159	(6+ Tf <sup>(+)</sup> ) - (5+TfH)	-41.7
6c	H <sup>+</sup> @N(1)	-4148.7592	0.0054	14.2	-5110.1829	6b+Tf <sup>(+)</sup>	-0.0011	(6b+ Tf <sup>(+)</sup> ) - (5+TfH)	-3.0
6d	H <sup>+</sup> @N(2)	-4148.7646			-4175.4795	5+BH <sub>4</sub> <sup>(-)</sup>			
					-4175.4024	6c+ $\frac{1}{2}$ B <sub>2</sub> H <sub>6</sub>			
					-4175.4079	6d+ $\frac{1}{2}$ B <sub>2</sub> H <sub>6</sub>	0.0716	(6d+ $\frac{1}{2}$ B <sub>2</sub> H <sub>6</sub> ) - (5+ BH <sub>4</sub> <sup>(-)</sup> )	188.0

Black colored numbers are used for generation of Figure 4 in the main text, whereas red colored numbers refer to structural isomers with higher energies.

**Scheme 1.** Isodesmic reaction for the determination of  $\alpha$ -peri-interaction energies ( $\alpha$ -PIEs).



$$AB + HH = E_1, AH + BH = E_2$$

Assuming the H··H, A··H, and B··H interactions to be energetically negligible, the AB-*peri*-interaction is attractive if  $E_1$  is energetically lower than  $E_2$  ( $E_{E1} < E_{E2}$ ), and repulsive if  $E_1$  is energetically higher than  $E_2$  ( $E_{E1} > E_{E2}$ ).

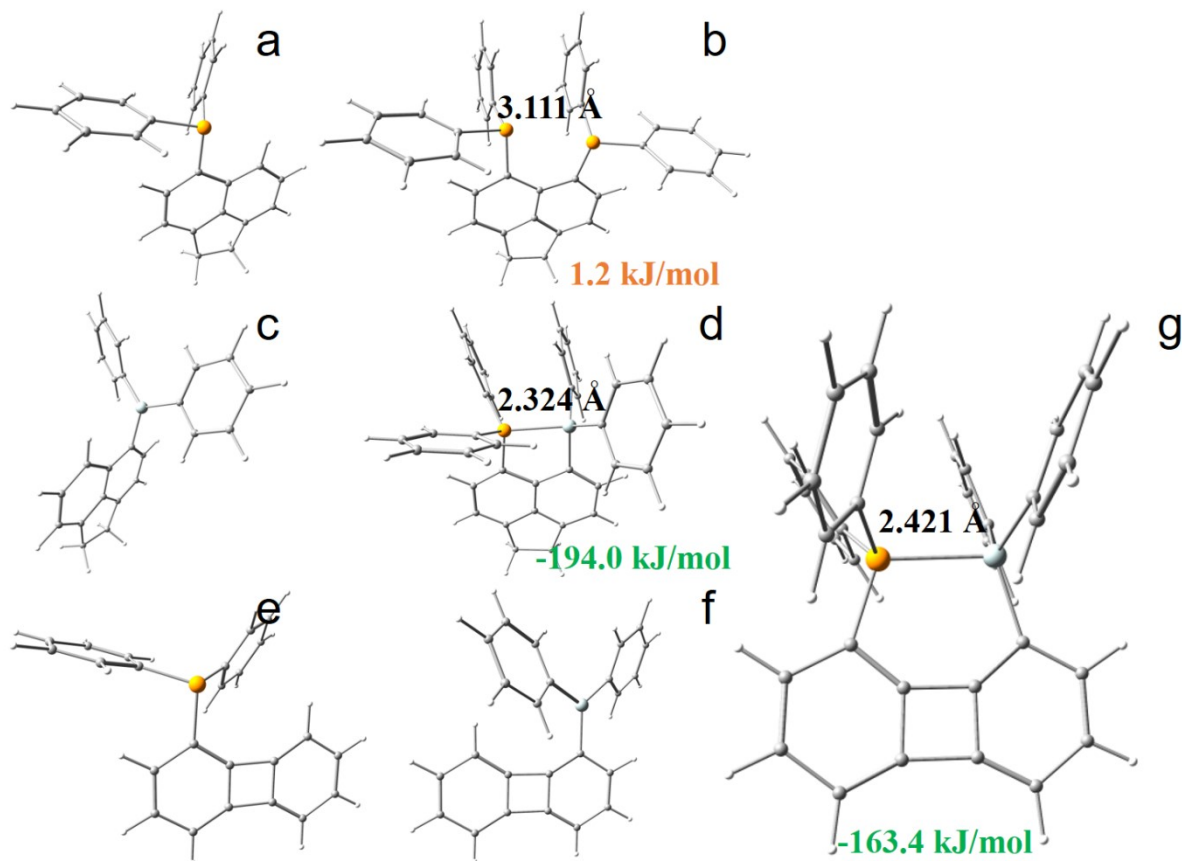


**Figure S6.** Fragments for estimation of the *peri*-interaction energy

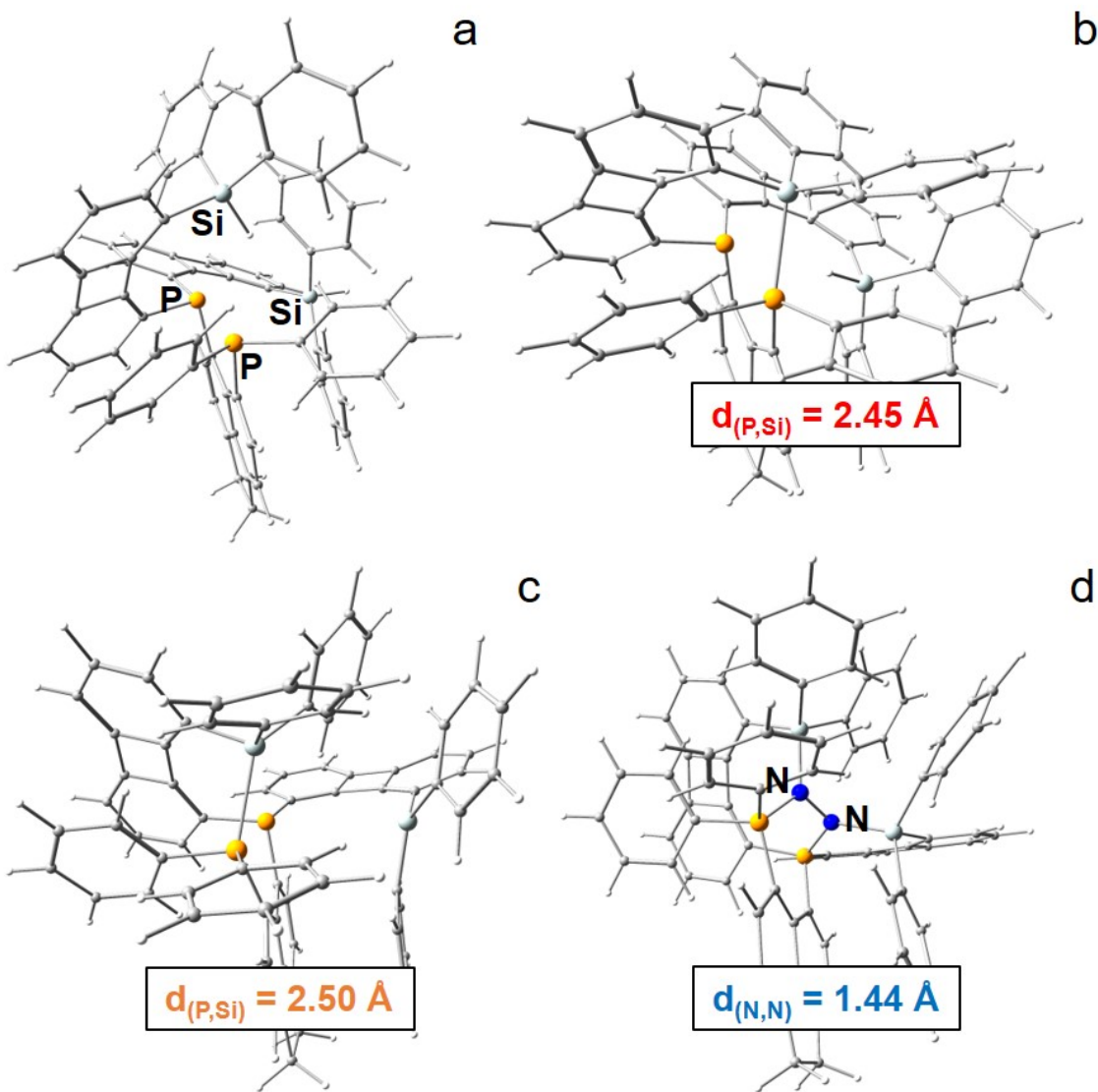


**Figure S7.** 3-spacer candidate employing acenaphthyl as spacer group for the LB part ( $-PPh_2$ ), but biphenylene (*bip*) for the LA part ( $-Ph_2Si^+$ ). (a) neutral molecule with two  $-SiHPh_2$  groups. (b) monocation with one  $-Ph_2Si^+$  group. (c) dication; active state. (d) N<sub>2</sub>-adduct exhibiting a PSiN-NSiP coordination mode. Si atoms are bluish-grey colored, P atoms orange, N atoms deep blue.

**Table S5.** Relevant geometric parameters for the 3-spacer approach ( $\text{\AA}$ ,  $^\circ$ ): *bip*-variant

state	P(1)-P(2)	P(1)-Si(1)	P(1)-Si(2)	P(2)-Si(1)	P(2)-Si(2)	Si(1)-Si(2)	N-N	$\Delta$
active	3.293	4.046	3.641	4.579	2.503	4.495		
N <sub>2</sub> -add.	3.292	3.149	3.938	3.838	3.150	3.913	1.437	0.347
state	Si(1)-N(1)	Si(2)-N(2)	P(1)-N(1)	P(2)-N(2)	Si(1)-N-N	Si(2)-N-N	P(1)-N-N	P(2)-N-N
N <sub>2</sub> -add.	1.861	1.834	1.689	1.696	116.98	117.14	114.05	116.19

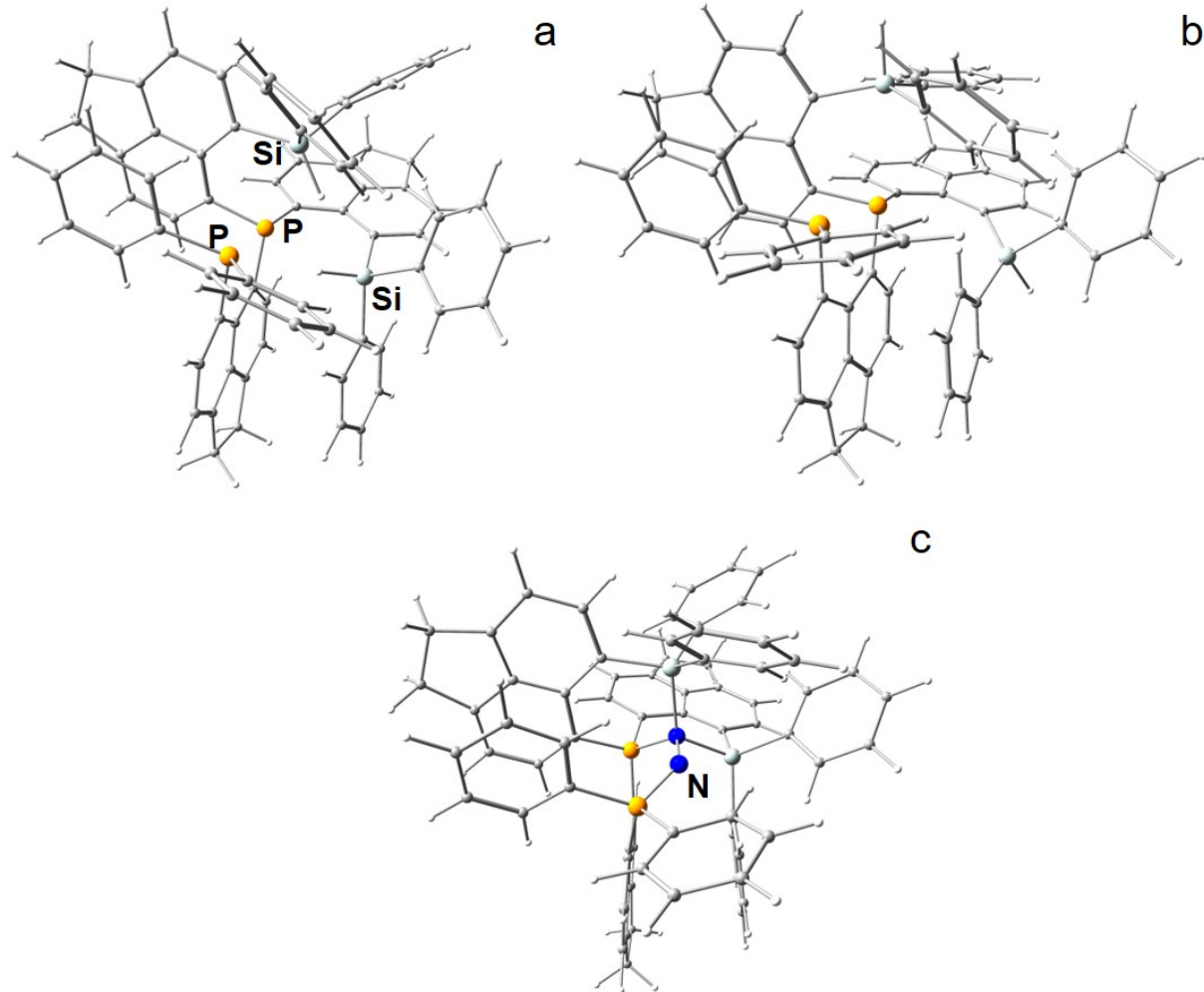


**Figure S8.** 3-spacer approach: Energetic disfavored structural isomers. (a) and (b) endo-endo- (**1a**) and exo-exo-version (**1b**) of the neutral ligand system, which are energetically disfavored against the endo-exo-version (**1c** = **1**, see Figure 2a in the main text). (c) P–N–N–Si<sub>2</sub>P coordination mode of the N<sub>2</sub>-adduct (**4c**).

**Table S6.** Geometric (Å, °) and energetic parameters of **3c**

state	P(1)-P(2)	P(1)-Si(2)	P(1)-Si(1)	P(2)-Si(2)	P(2)-Si(1)	Si(1)-Si(2)	N-N	Δ
N <sub>2</sub> (v3)-add state	3.262	2.950	3.084	3.965	3.854	3.373	1.442	0.351
	Si(2)-N(1)	Si(1)-N(1)	P(1)-N(1)	P(2)-N(2)	Si(2)-N-N	Si(1)-N-N	P(1)-N-N	P(2)-N-N
N <sub>2</sub> (v3)-add	1.927	1.951	1.756	1.602	101.60	99.37	116.03	129.79

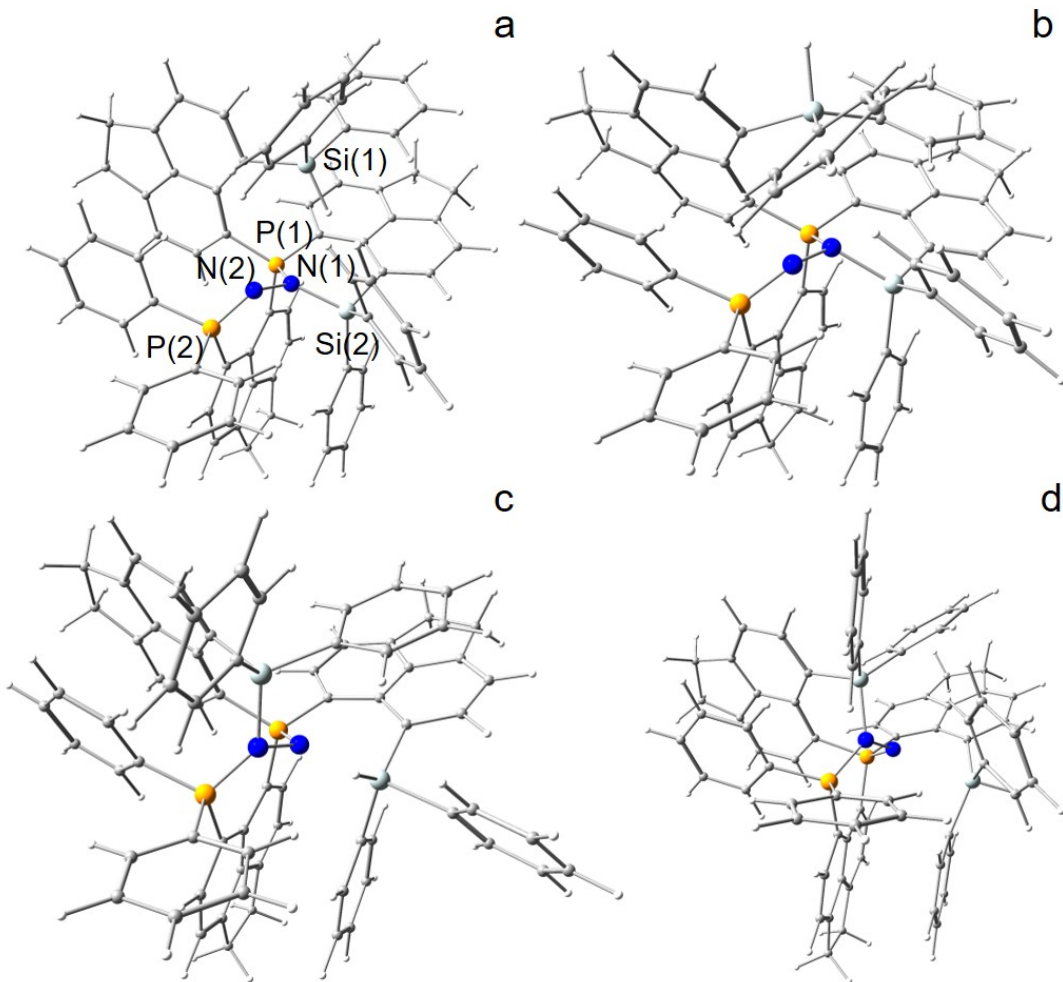


**Figure S9.** 3-spacer approach: Hydride formation of the PSiN–NSiP N<sub>2</sub>-adduct at the Si sites. (a) Si(1)-endo (**5c**). (b) Si(1)-exo (**5d**). (c) Si(2)-endo (**5e**). (d) Si(2)-exo (**5f**).

**Table S7.** Geometric (Å, °) and energetic parameters of adding hydride to Si at the N<sub>2</sub>-adduct

state	d(Si(2)-N(1))	d(Si(1)-N(2))	d(P(1)-N(1))	d(P(2)-N(2))	d(N(1)-N(2))
<b>5c</b> Si(1)-endo	1.762	3.768	1.641	1.601	1.424
<b>5d</b> Si(1)-exo	1.784	3.568	1.649	1.595	1.425
<b>5e</b> Si(2)-endo	2.144	1.783	1.607	1.653	1.422
<b>5f</b> Si(2)-exo	2.653	1.796	1.610	1.662	1.442
state	Si(2)-N(1)-N(2)	Si(1)-N(2)-N(1)	P(1)-N(1)-N(2)	P(2)-N(2)-N(1)	ΔE (kJ mol <sup>-1</sup> )
<b>5c</b> Si(1)-endo	120.6	63.8	118.3	117.4	75.2
<b>5d</b> Si(1)-exo	114.2	71.5	118.8	124.6	104.3
<b>5e</b> Si(2)-endo	115.5	102.2	117.0	118.6	122.1
<b>5f</b> Si(2)-exo	129.6	102.5	114.3	118.0	153.7

ΔE refers to the N<sub>2</sub>-adduct. Si–H bond formation is energetically adverse.

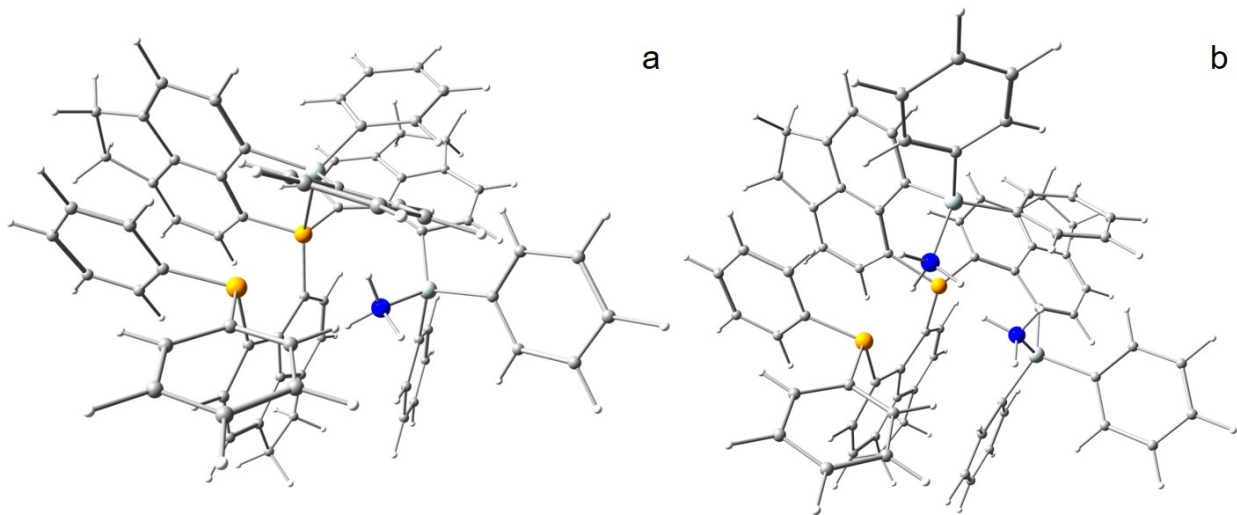


**Figure S10.** NH<sub>3</sub>-poisoned states **3a**•NH<sub>3</sub> and **3a**•2NH<sub>3</sub> at the b3pw91-D3/6-31+G\* level.

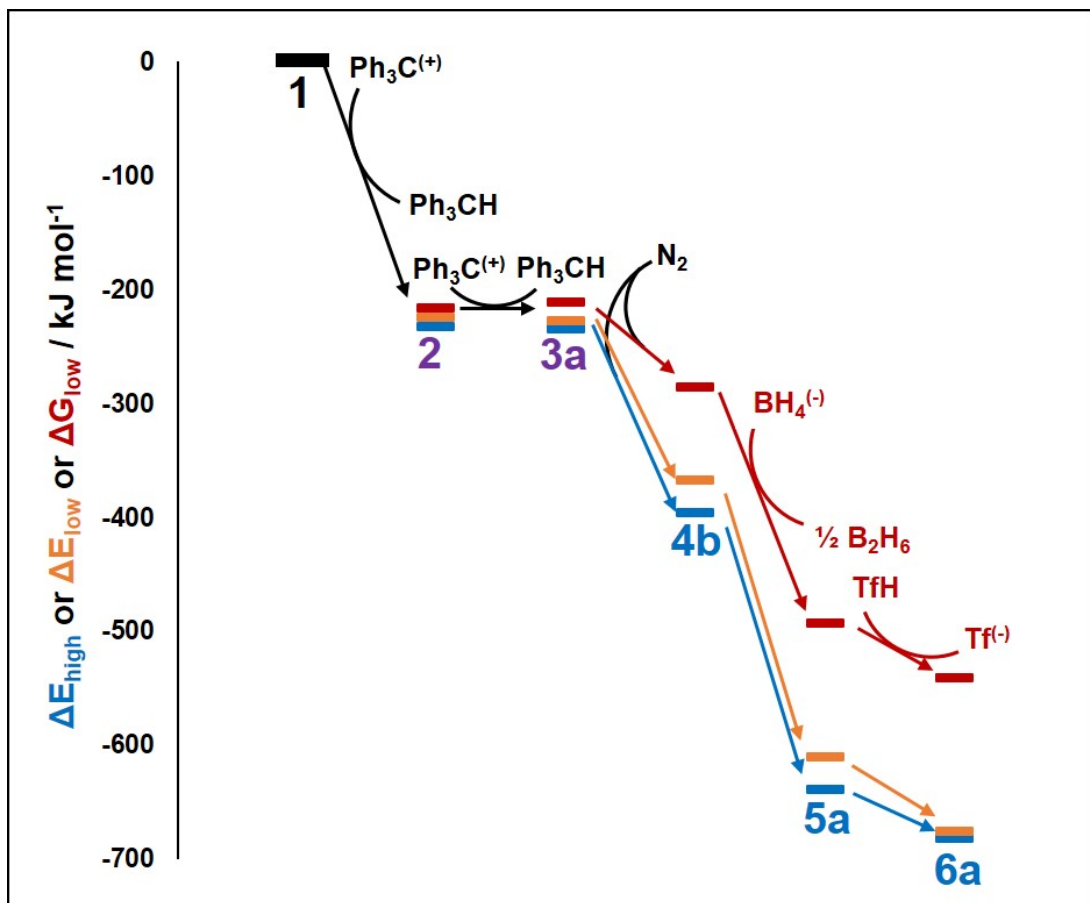


**Figure S11.** ΔE<sub>high</sub> (b3pw91-D3/6-311+G(2df,p)) and ΔE<sub>low</sub> of ΔG<sub>low</sub> (b3pw91-D3/6-31+G\*) energy diagrams of the investigated reactions steps. Details are given for ΔG<sub>low</sub>. See also Figure 4 in the main text.

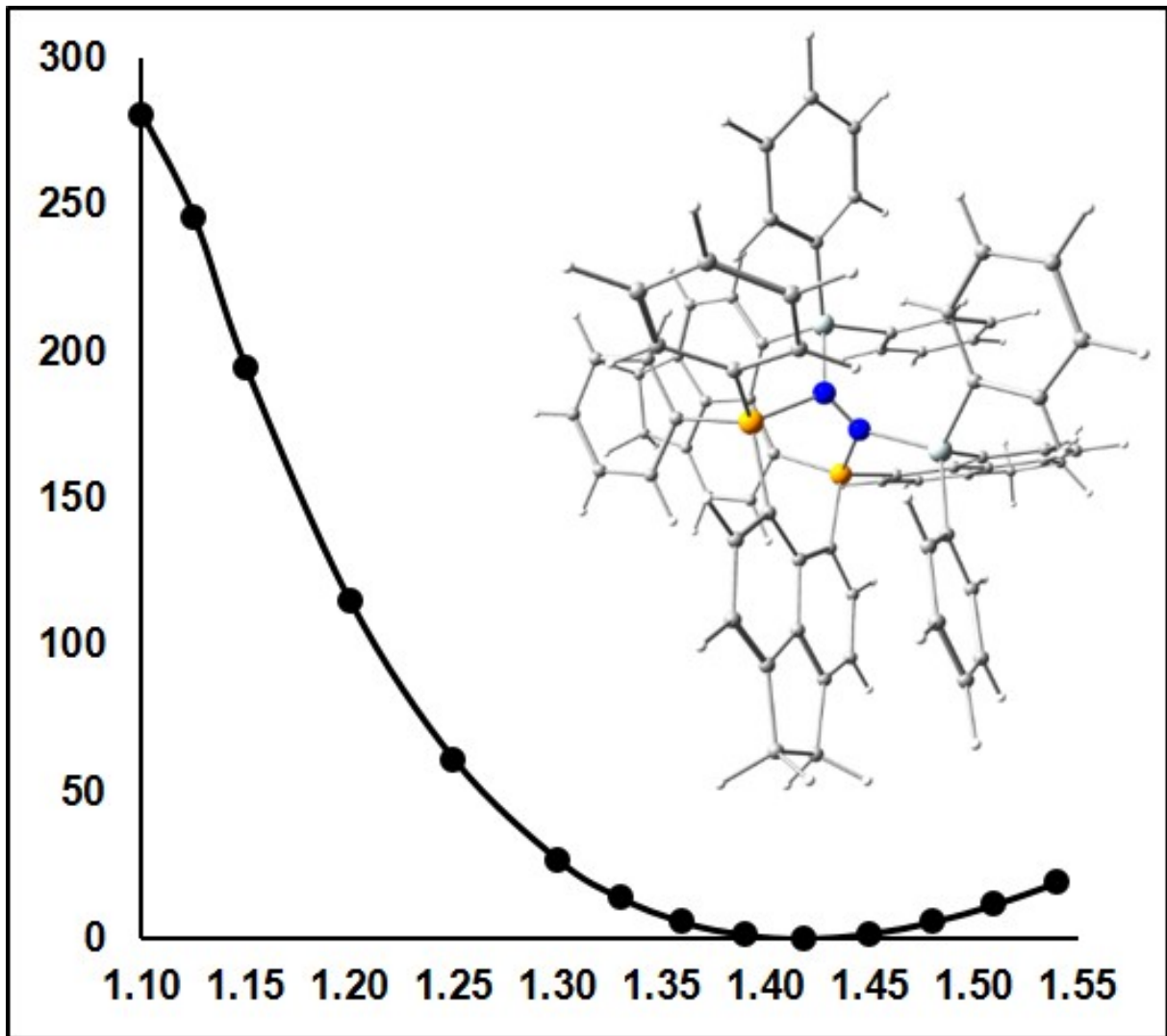


**Figure S12.** Potential energy scan (PES) of **4b** with fixed N–N distances varying from 1.10–1.55 Å at the b3pw91-D3/6-31+G\* level of theory (gas-phase). The PES shows that once N<sub>2</sub> has entered the “active site” of the dication, N–N bond elongation to about 1.42 Å don’t has to overcome an activation barrier. The displayed molecular structure refers to the optimized coordinates of the model with a N–N bond distance of 1.10 Å.

**Table S8.** Geometric ( $\text{\AA}$ ,  $^\circ$ ) parameters for DFT-calculations at different basis-set size.

	<b>1<sub>low</sub></b>	<b>1<sub>high</sub></b>	<b>2<sub>low</sub></b>	<b>2<sub>high</sub></b>	<b>3a<sub>low</sub></b>	<b>3a<sub>high</sub></b>	<b>3b<sub>low</sub></b>	<b>3b<sub>high</sub></b>		
	<b>4a<sub>low</sub></b>	<b>4a<sub>high</sub></b>	<b>4b<sub>low</sub></b>	<b>4b<sub>high</sub></b>	<b>4c<sub>low</sub></b>	<b>4c<sub>high</sub></b>	<b>5<sub>low</sub></b>	<b>5<sub>high</sub></b>	<b>6<sub>low</sub></b>	<b>6<sub>high</sub></b>
P(1)-P(2)	3.035	3.026	3.103	3.083	3.188	3.180	3.067	3.061		
P(1)-Si(1)	3.346	3.332	2.365	2.361	2.400	2.393	2.437	2.428		
P(1)-Si(2)	3.305	3.292	3.416	3.393	3.067	3.056	3.472	3.435		
P(2)-Si(1)	4.122	4.108	3.271	3.265	3.640	3.623	3.357	3.336		
P(2)-Si(2)	4.494	4.491	4.771	4.688	4.621	4.609	4.688	4.697		
Si(1)-Si(2)	5.233	5.194	3.984	3.960	4.451	4.426	4.202	4.174		
P(1)-P(2)	2.917	2.901	3.338	3.326	3.270	3.262	3.548	3.540	3.718	3.692
P(1)-Si(1)	3.477	3.469	3.224	3.206	3.084	3.085	3.186	3.168	3.171	3.167
P(1)-Si(2)	3.438	3.427	3.892	3.873	2.968	2.950	4.708	4.668	5.138	5.109
P(2)-Si(1)	3.740	3.730	3.425	3.414	3.869	3.852	3.790	3.785	3.868	3.871
P(2)-Si(2)	3.926	3.908	2.994	2.979	3.964	3.966	2.962	2.945	2.939	2.922
Si(1)-Si(2)	3.310	3.288	3.941	3.920	3.399	3.372	4.584	4.552	4.910	4.914
P(1)-N	1.699	1.688	1.701	1.686	1.774	1.756	1.567	1.556	1.638	1.624
P(2)-N	1.705	1.692	1.674	1.662	1.617	1.602	1.630	1.617	1.679	1.662
Si(1)-N	1.786	1.775	1.832	1.821	1.959	1.951	1.699	1.689	1.767	1.757
Si(2)-N	1.793	1.782	1.799	1.790	1.938	1.927	1.753	1.740	1.803	1.792
N(1)-N(2)	1.415	1.417	1.416	1.418	1.447	1.442	2.608	2.596	2.694	2.722
N(1)-H									1.030	1.024
N(2)-H							1.043	1.046	1.024	1.022
P(1)-N-N	115.66	115.29	113.11	113.36	117.01	115.96	103.89	103.27	122.35	120.68
P(2)-N-N	125.84	125.99	116.26	115.96	127.74	129.96	96.26	97.02	87.48	87.09
Si(1)-N-N	110.77	110.95	106.77	106.68	101.52	99.02	91.72	92.09	92.90	92.91
Si(2)-N-N	109.63	109.97	124.20	124.27	99.49	101.89	137.11	136.54	136.03	135.99

“low” refers to calculations at the b3pw91-D3/6-31+G\* level.

“high” refers to calculations at the B3PW91-D3/6-311+G(2df,p) level.

**Table S9.** Thermodynamic properties of relevant states

model	1	2	3a	3b	4a	4b	4c	5a	6a
E	-4038.454	-4037.737	-4036.936	-4036.936	-4146.458	-4146.472	-4146.435	-4147.263	-4147.705
ZPE-corr (H/n)	1.063	1.057	1.049	1.050	1.062	1.062	1.061	1.069	1.084
TD-E corr	1.125	1.119	1.109	1.111	1.124	1.124	1.123	1.132	1.146
TD-H corr	1.126	1.119	1.110	1.112	1.124	1.125	1.124	1.133	1.147
TD-G corr	0.966	0.962	0.958	0.956	0.969	0.970	0.966	0.972	0.988
E+ZPE	-4037.391	-4036.680	-4035.887	-4035.860	-4145.396	-4145.410	-4145.374	-4146.194	-4146.621
E+TD-E	-4037.329	-4036.619	-4035.827	-4035.799	-4145.334	-4145.348	-4145.312	-4146.131	-4146.559
E+TD-H	-4037.328	-4036.618	-4035.826	-4035.798	-4145.334	-4145.347	-4145.311	-4146.130	-4146.558
E+TD-G	-4037.488	-4036.775	-4035.978	-4035.953	-4145.489	-4145.502	-4145.468	-4146.291	-4146.717
E-TD (Kcal/mol)	705.947	701.886	696.031	697.163	705.028	705.086	704.733	710.484	719.275
CV (Cal/molK)	254.436	252.194	248.479	250.695	254.120	254.146	255.059	256.724	257.635
S (Cal/molK)	335.632	331.090	319.696	327.198	327.544	324.617	331.611	339.507	335.437
model	BH <sub>3</sub>	B <sub>2</sub> H <sub>6</sub>	½ B <sub>2</sub> H <sub>6</sub>	BH <sub>4</sub> <sup>(*)</sup>	N <sub>2</sub>	CPh <sub>3</sub>	CPh <sub>3</sub> H	Tf <sup>(*)</sup>	TfH
E	-26.599	-53.287	-26.643	-27.342	-109.483	-732.689	-733.491	-961.380	-961.797
ZPE-corr (H/n)	0.026	0.063	0.032	0.034	0.006	0.282	0.292	0.027	0.038
TD-E corr	0.029	0.067	0.033	0.037	0.008	0.296	0.307	0.034	0.046
TD-H corr	0.030	0.068	0.034	0.038	0.009	0.297	0.308	0.035	0.047
TD-G corr	0.009	0.041	0.020	0.016	-0.013	0.240	0.247	-0.005	0.005
E+ZPE	-26.572	-53.208	-26.604	-27.308	-109.477	-732.407	-733.199	-961.354	-961.759
E+TD-E	-26.570	-53.204	-26.602	-27.305	-109.475	-732.392	-733.184	-961.346	-961.751
E+TD-H	-26.569	-53.203	-26.602	-27.304	-109.474	-732.392	-733.183	-961.345	-961.750
E+TD-G	-26.590	-53.230	-26.615	-27.326	-109.495	-732.449	-733.244	-961.385	-961.793
E-TD (Kcal/mol)	18.259	41.907	20.954	23.009	5.014	185.920	192.588	21.369	28.934
CV (Cal/molK)	6.641	11.399	5.700	7.260	4.970	59.111	60.046	24.547	26.871
S (Cal/molK)	45.030	56.903		45.236	45.780	121.477	128.569	83.272	88.75

Calculations at the b3pw91-D3/6-31+G\* level.

**Table S10.**  $\Delta E$  and  $\Delta G$  values for state transitions displayed in Figure 4 in  $\text{kJ mol}^{-1}$ 

step	$\Delta E_{\text{high}}$	$\Delta E_{\text{low}}$	$\Delta G_{\text{low}}$
<b>1 → 2</b>	-232.1	-224.3	-216.6
<b>2 → 3a</b>	-2.6	-3.0	5.8
<b>2 → 3b</b>	59.6	64.9	69.3
<b>3a → 4a</b>	-125.5	-103.6	-42.1
<b>3a → 4b</b>	-161.6	-140.3	-74.9
<b>3a → 4c</b>	-61.8	-42.6	12.6
<b>4b → 5</b>	-242.6	-243.1	-207.5
<b>5 → 6</b>	-43.3	-64.5	-47.5

“low” refers to calculations at the b3pw91-D3/6-31+G\* level.

“high” refers to calculations at the b3pw91-D3/6-311+G(2df,p) level.

**Table S11.** AIM atomic charges of dinitrogen, diazene, hydrazine, and ammonia

	N <sub>2</sub>	N <sub>2</sub> H <sub>2</sub>	N <sub>2</sub> H <sub>4</sub>	NH <sub>3</sub>
$\frac{Q_{(\text{AIM})} [\text{e}]}{d_{(\text{N-N})} [\text{\AA}]}$	1.091	1.223	1.428	
N(1)	0.00	-0.33	-0.68	-1.04
N(2)	0.00	-0.33	-0.68	
H(1)		0.34	0.35	0.35
H(2)		0.33	0.35	0.35
H(3)			0.34	0.35
H(4)			0.34	
$\Sigma$	0.01	0.01	0.02	0.01

**Table S12.** ELI-D properties of the lone-pair basins

LP(N)	no.	N <sub>ELI</sub> [e]	V <sub>ELI</sub> [Å <sup>3</sup> ]	γ <sub>ELI</sub>	RJI	hybrid.	comment
N <sub>2</sub>		3.14	30.2	1.90		"sp"	
N <sub>2</sub> H <sub>2</sub>		2.63	24.4	2.02		"sp <sup>2</sup> "	
N <sub>2</sub> H <sub>4</sub>		2.18	16.4	1.92		"sp <sup>3</sup> "	
NH <sub>3</sub>		2.14	26.4	1.73		"sp <sup>3</sup> "	
<b>5a</b>	N(2)	2.90	8.6	1.54	99.1	Si-N-P	NSiP
<b>4b</b>	N(2)	1.94	5.1	1.78	99.6	"sp <sup>3</sup> "	NSiP
<b>6a</b>	N(1)	1.88	5.4	1.72		"sp <sup>3</sup> "	NSiP
<b>4a</b>	N(1)	1.71	4.4	1.73	99.4	"sp <sup>3</sup> "	NSi <sub>2</sub>
<b>4a</b>	N(2)	1.67	3.6	1.69	99.8	"sp <sup>2</sup> "	NP <sub>2</sub>
<b>5a</b>	N(1)	1.62	5.0	1.64	99.7	"sp <sup>2</sup> "	NSiP
<b>4b</b>	N(1)	1.61	3.6	1.70	99.8	"sp <sup>2</sup> "	NSiP
<b>6a</b>	N(2)	1.32	4.5	1.60		"sp <sup>2</sup> "	NSiP
<b>4a</b>	N(2)	1.27	2.7	1.61	99.7	"sp <sup>2</sup> "	NP <sub>2</sub>

**Table S13.** Topological and integrated RSBIs of the Si–N and P–N bonds

Si–N	d [Å]	ρ(r) <sub>bcp</sub> [eÅ <sup>-3</sup> ]	∇ <sup>2</sup> ρ(r) <sub>bcp</sub> [eÅ <sup>-5</sup> ]	ε	d <sub>l</sub> /d	RJI	G/ρ(r) [a.u.]	H/ρ(r) [a.u.]	G/V	N <sub>ELI</sub> [e]	V <sub>ELI</sub> [Å <sup>3</sup> ]	γ <sub>ELI</sub>
<b>4b</b>	1.821	0.74	8.5	0.12	0.39	93.9	1.32	-0.52	0.72	2.46	4.8	1.75
<b>6a</b>	1.792	0.78	9.5	0.08	0.40	94.0	1.38	-0.53	0.72	2.72	5.9	1.69
<b>4b</b>	1.790	0.78	9.6	0.13	0.40	94.5	1.39	-0.52	0.73	2.85	5.6	1.73
<b>4a</b>	1.782	0.82	10.1	0.15	0.40	92.1	1.41	-0.54	0.72	2.23	4.6	1.74
<b>4a</b>	1.775	0.83	10.1	0.15	0.40	92.4	1.41	-0.55	0.72	2.27	4.3	1.73
<b>6a</b>	1.757	0.82	11.2	0.08	0.40	93.0	1.48	-0.52	0.74	2.10	4.1	1.71
<b>5a</b>	1.740	0.86	11.7	0.08	0.40	92.9	1.50	-0.54	0.73	2.32	5.0	1.68
<b>5a</b>	1.689	0.92	15.2	0.02	0.41	92.7	1.68	-0.53	0.76	2.56	5.7	1.59
P–N	d [Å]	ρ(r) <sub>bcp</sub> [eÅ <sup>-3</sup> ]	∇ <sup>2</sup> ρ(r) <sub>bcp</sub> [eÅ <sup>-5</sup> ]	ε	d <sub>l</sub> /d	RJI	G/ρ(r) [a.u.]	H/ρ(r) [a.u.]	G/V	N <sub>ELI</sub> [e]	V <sub>ELI</sub> [Å <sup>3</sup> ]	γ <sub>ELI</sub>
<b>4a</b>	1.692	1.20	4.4	0.18	0.39	81.2	1.22	-0.96	0.56	1.62	2.5	1.65
<b>4a</b>	1.688	1.22	4.7	0.16	0.39	83.4	1.25	-0.97	0.56	1.72	2.5	1.68
<b>4b</b>	1.686	1.24	3.9	0.19	0.39	82.5	1.21	-0.99	0.55	1.79	2.6	1.67
<b>6a</b>	1.662	1.28	5.3	0.10	0.39	82.0	1.29	-0.99	0.56	1.97	3.2	1.62
<b>4b</b>	1.662	1.29	5.8	0.19	0.39	81.7	1.31	-0.99	0.57	1.84	2.9	1.66
<b>6a</b>	1.624	1.34	9.0	0.15	0.39	82.0	1.45	-0.98	0.60	1.92	3.0	1.64
<b>5a</b>	1.617	1.38	8.8	0.13	0.39	83.1	1.45	-1.00	0.59	2.02	3.0	1.61
<b>5a</b>	1.556	1.48	16.1	0.03	0.40	81.8	1.74	-0.98	0.64	2.23	3.9	1.53

ρ(r)<sub>bcp</sub>: ED at the bcp, ∇<sup>2</sup>ρ(r)<sub>bcp</sub>: Laplacian, ε: bond ellipticity d<sub>l</sub>: distance atom(1)-bcp, RJI: Raub-Jansen Index, G/ρ(r)<sub>bcp</sub>, H/ρ(r)<sub>bcp</sub>: kinetic and total energy density over ρ(r)<sub>bcp</sub> ratios, V: potential energy density, N<sub>ELI</sub>, V<sub>ELI</sub>: electron populations and volumes the ELI-D basin, γ<sub>ELI</sub>: ELI-D value at the attractor position.

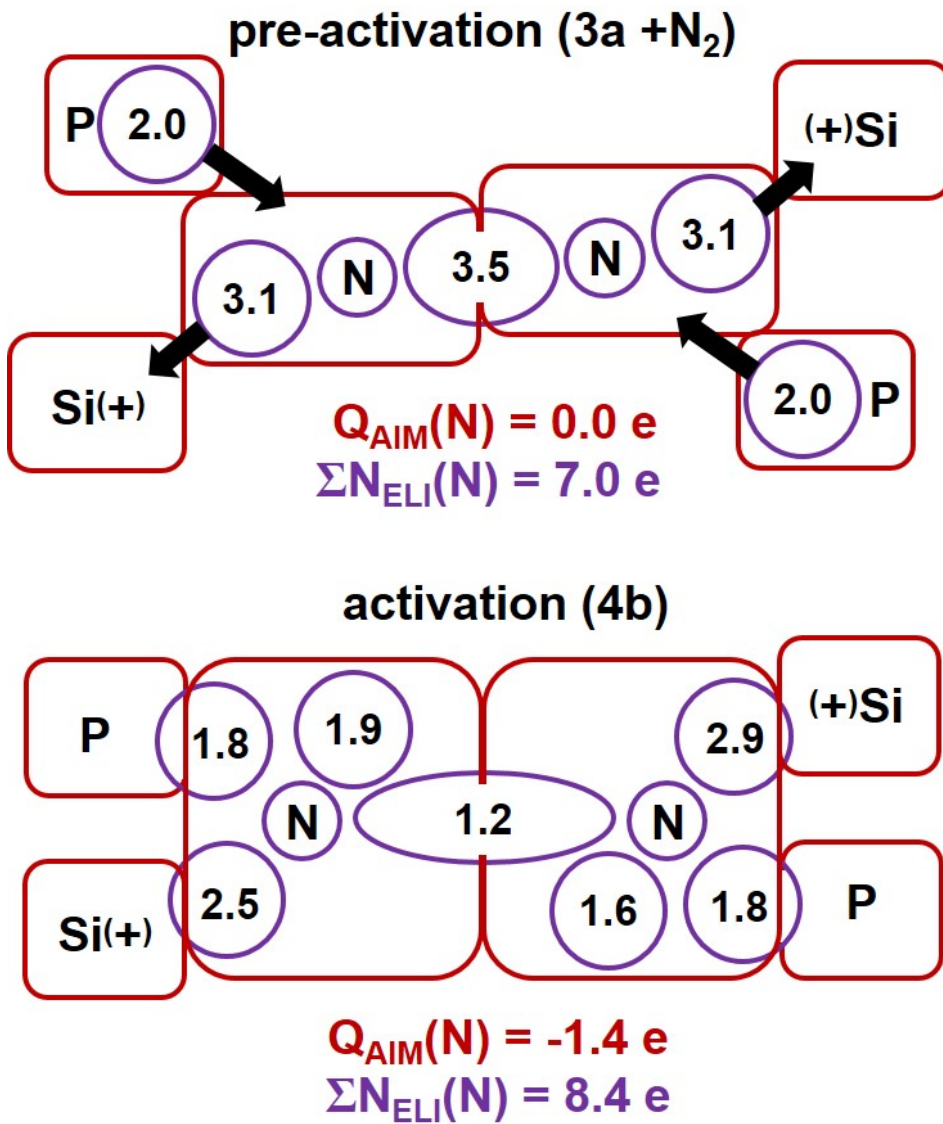


**Figure S13.** Combination of AIM atomic basins (red) and ELI-D basins (purple). In the process of N<sub>2</sub>-uptake and –activation the N≡N ELI-D basin (V<sub>2</sub>(N,N)) loses significant amounts of electron population, which is directed towards the newly formed lone pair basins (V<sub>1</sub>(N), LP(N)) of the N<sub>2</sub>-adduct. The newly formed Si–N basins stem from the LP(N) basins in N<sub>2</sub>. The newly formed P–N basins stem from the LP(P) basins of the ligand system. Since the RJI is larger than 80% for the P–N basins and larger than 90% for the Si–N basins, the AIM atomic charges of the N atoms become significantly negative, despite all ELI-basins seemingly loose electron population. Core basins (C(N)) contain 2.1 e. Black arrows indicate direction of donor-acceptor bond formation.

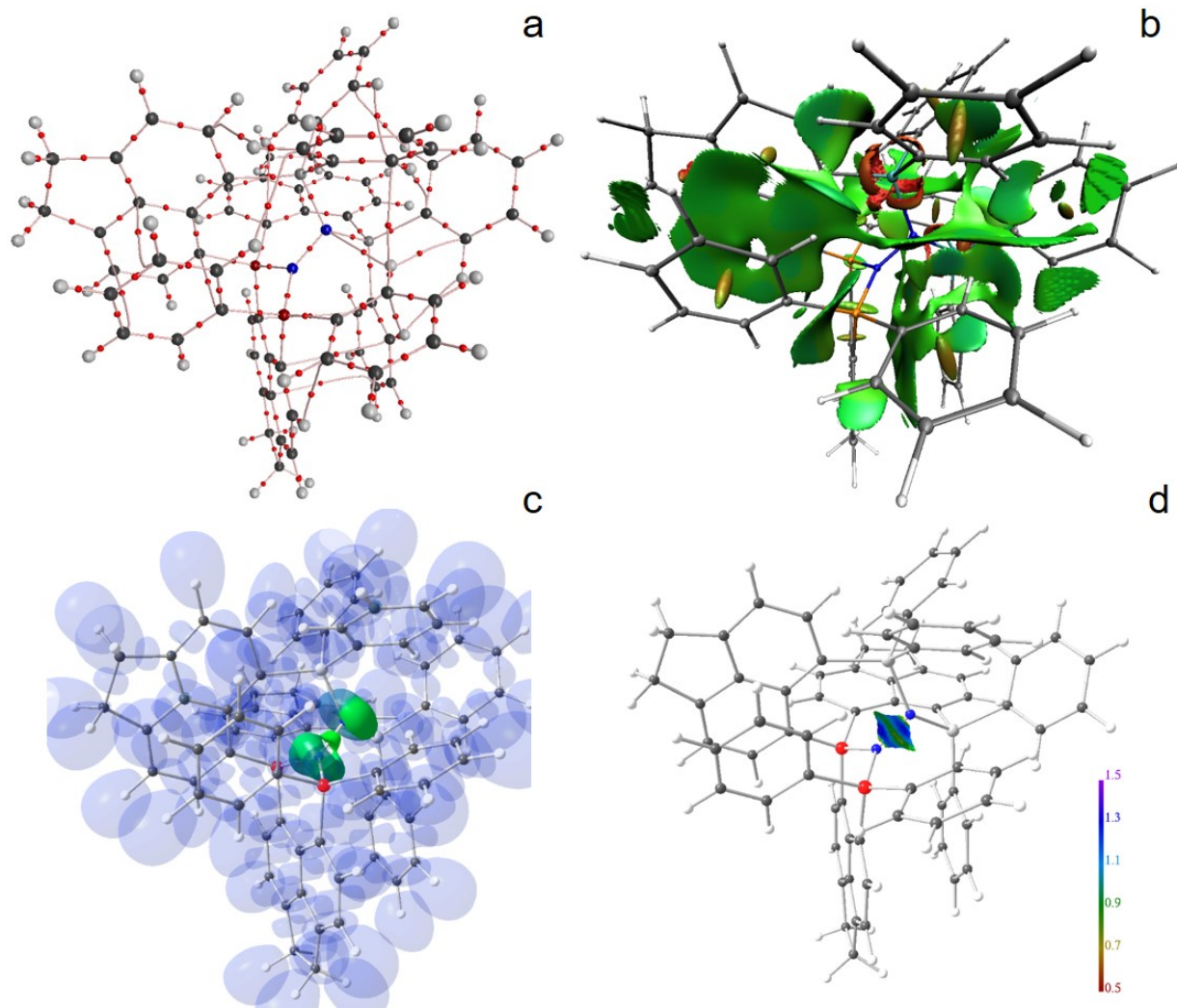


**Figure S14.** RSBI analysis of **4a** (a) AIM bond paths motif, (b) NCI *iso*-surface at  $s(\mathbf{r}) = 0.5$ , (c) ELI-D localization domain representation at *iso*-value of 1.35, (d) ELI-D distribution mapped on the N–N ELI-D bonding basin. Full molecule representation. Atom colors: P (red or orange), Si (light gray or light blue), N (blue), C (dark grey).

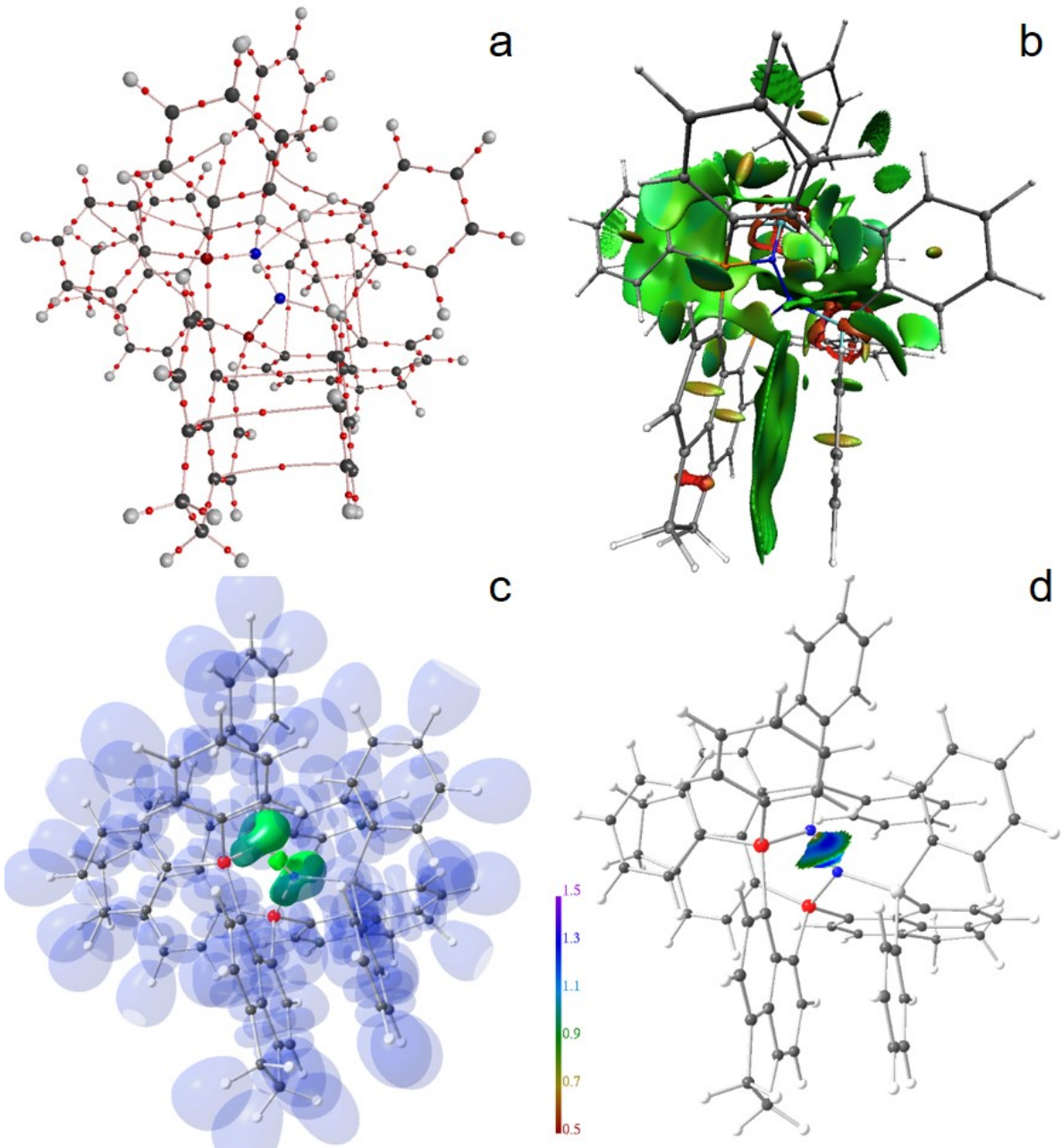


**Figure S15.** RSBI analysis of **4b** (a) AIM bond paths motif, (b) NCI *iso*-surface at  $s(\mathbf{r}) = 0.5$ , (c) ELI-D localization domain representation at *iso*-value of 1.35, (d) ELI-D distribution mapped on the N–N ELI-D bonding basin. Full molecule representation. Atom colors: P (red or orange), Si (light gray or light blue), N (blue), C (dark grey).

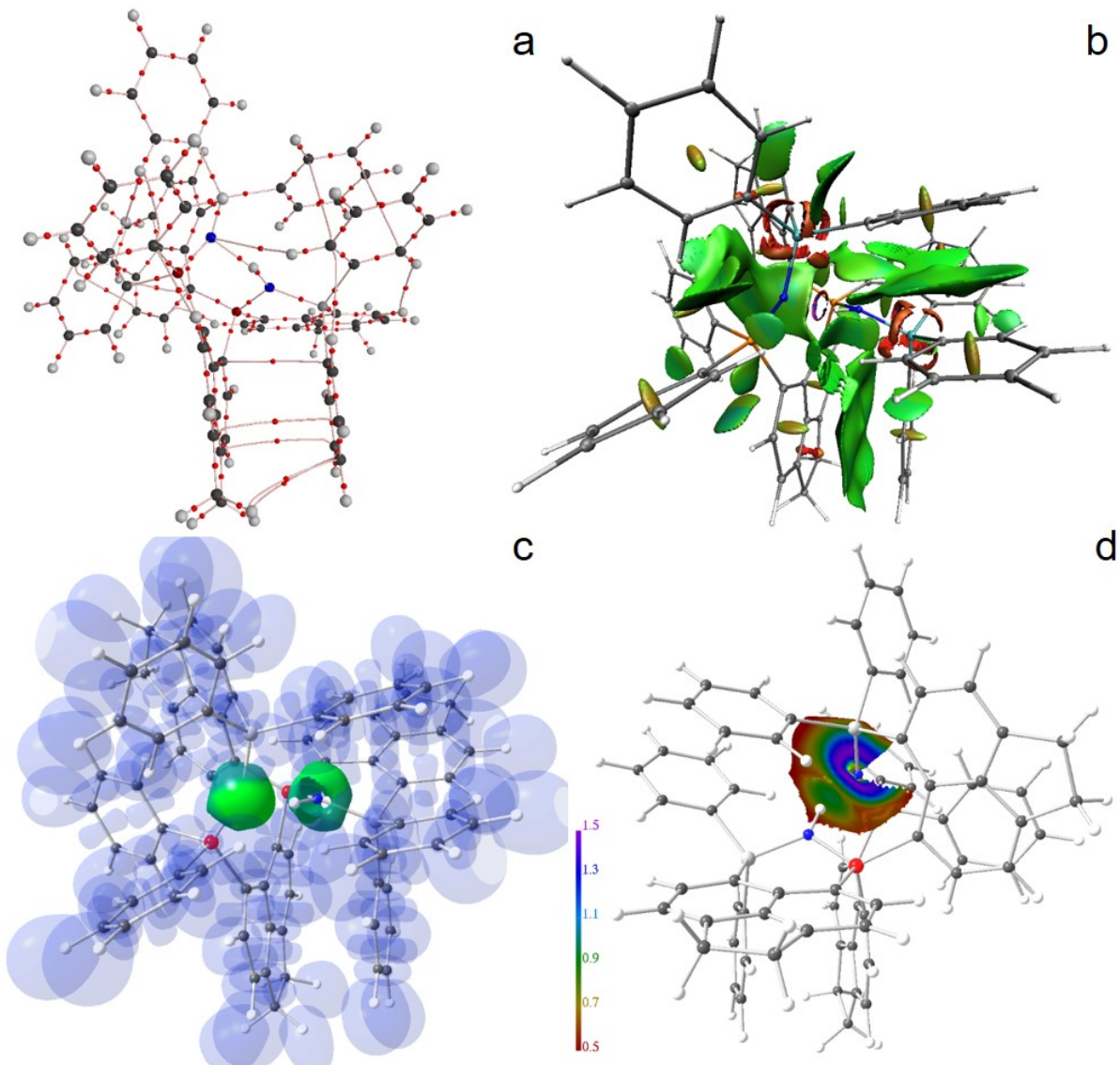


**Figure S16.** RSBI analysis of **5a** (a) AIM bond paths motif, (b) NCI *iso*-surface at  $s(\mathbf{r}) = 0.5$ , (c) ELI-D localization domain representation at *iso*-value of 1.35, (d) ELI-D distribution mapped on the N–N ELI-D bonding basin. Full molecule representation. Atom colors: P (red or orange), Si (light gray or light blue), N (blue), C (dark grey).

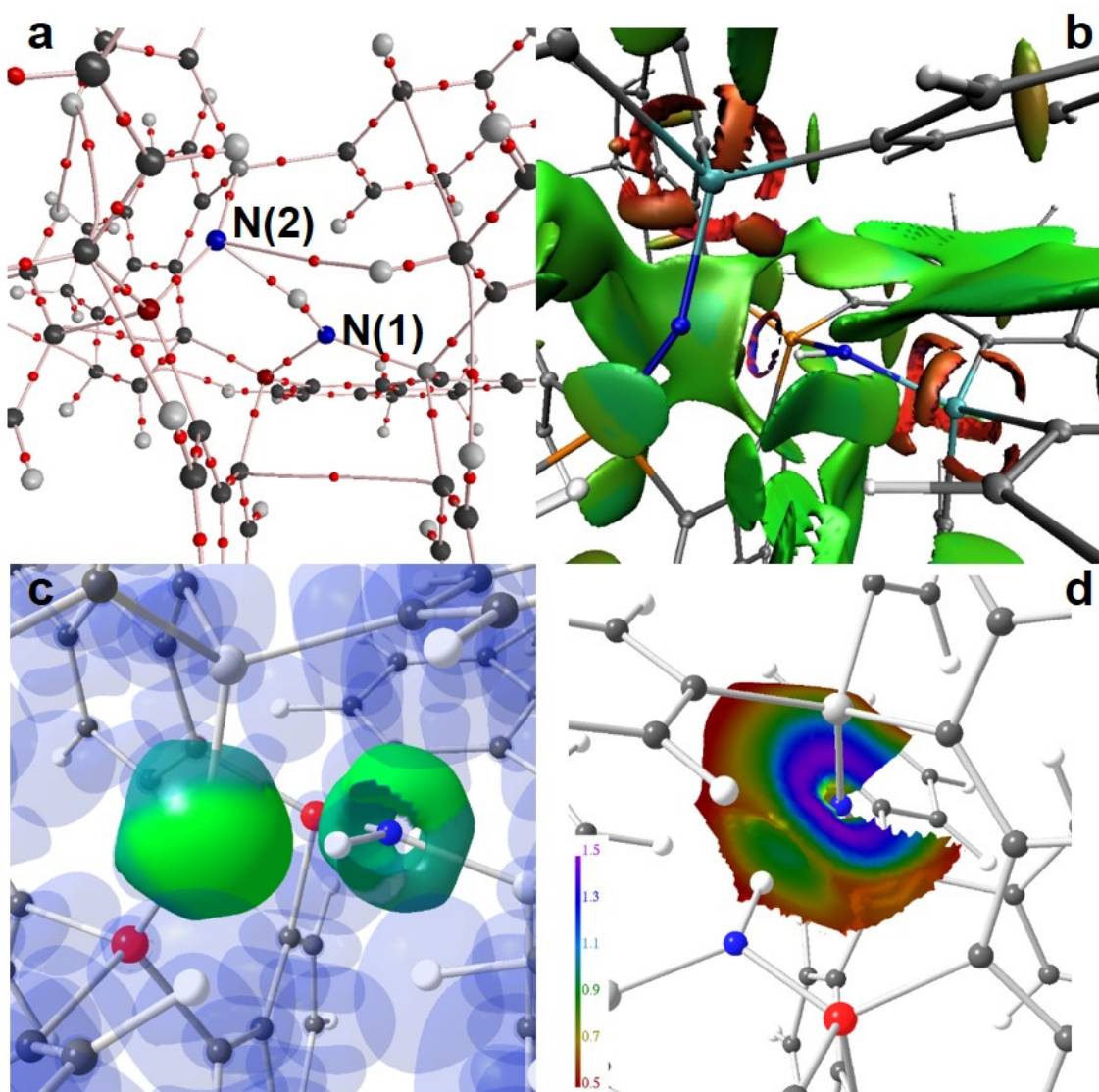


**Figure S17.** RSBI analysis of **5a** (a) AIM bond paths motif, (b) NCI *iso*-surface at  $s(\mathbf{r}) = 0.5$ , (c) ELI-D localization domain representation at *iso*-value of 1.35, (d) ELI-D distribution mapped on the N–N ELI-D bonding basin. For clarity, the orientation of the view was changed to highlight the N–H···N contact. Magnification of the active site. Atom colors: P (red or orange), Si (light gray or light blue), N (blue), C (dark grey).

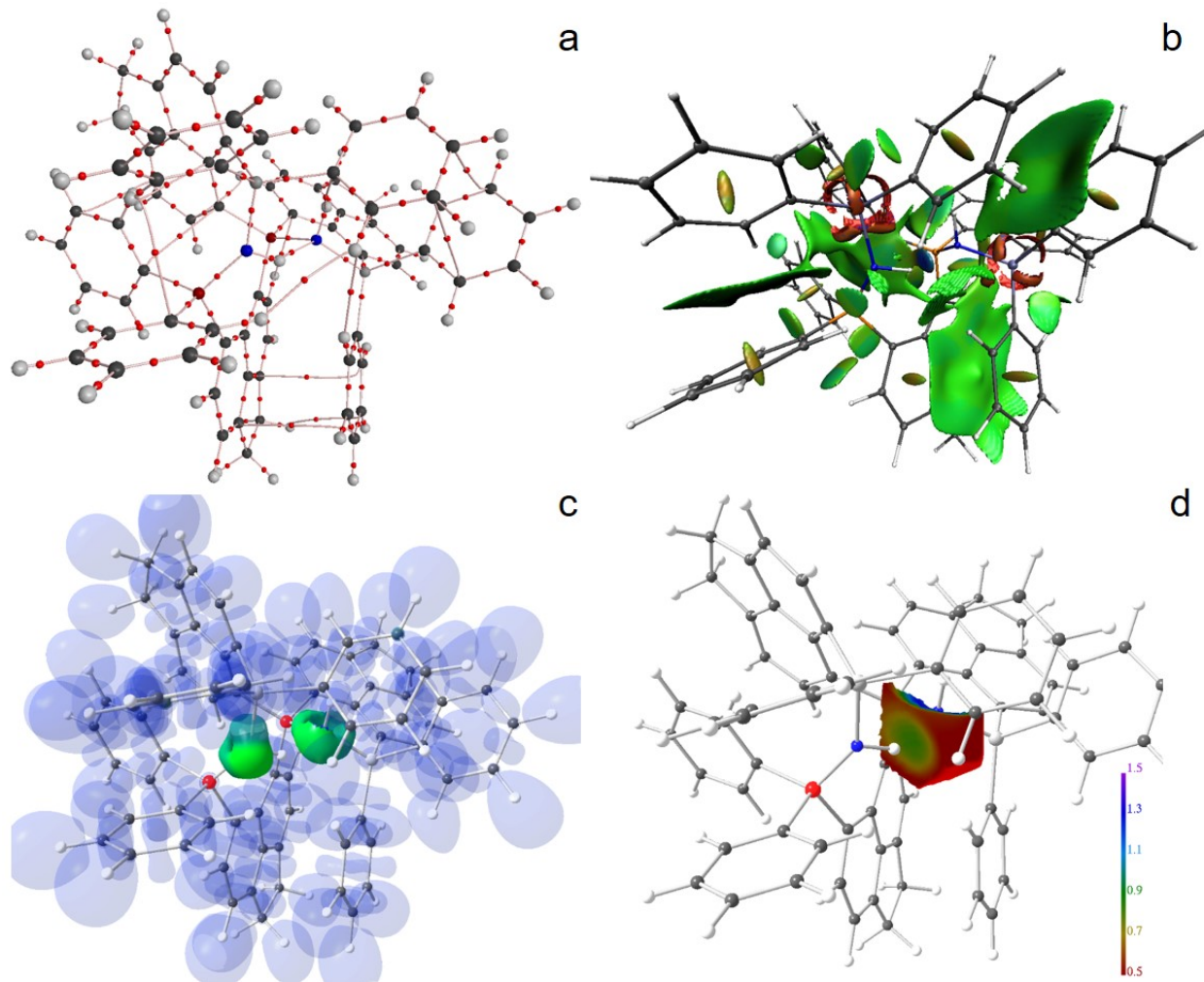


**Figure S18.** RSBI analysis of **6a** (a) AIM bond paths motif, (b) NCI *iso*-surface at  $s(\mathbf{r}) = 0.5$ , (c) ELI-D localization domain representation at *iso*-value of 1.35, (d) ELI-D distribution mapped on the N–N ELI-D bonding basin. Full molecule representation. Atom colors: P (red or orange), Si (light gray or light blue), N (blue), C (dark grey).

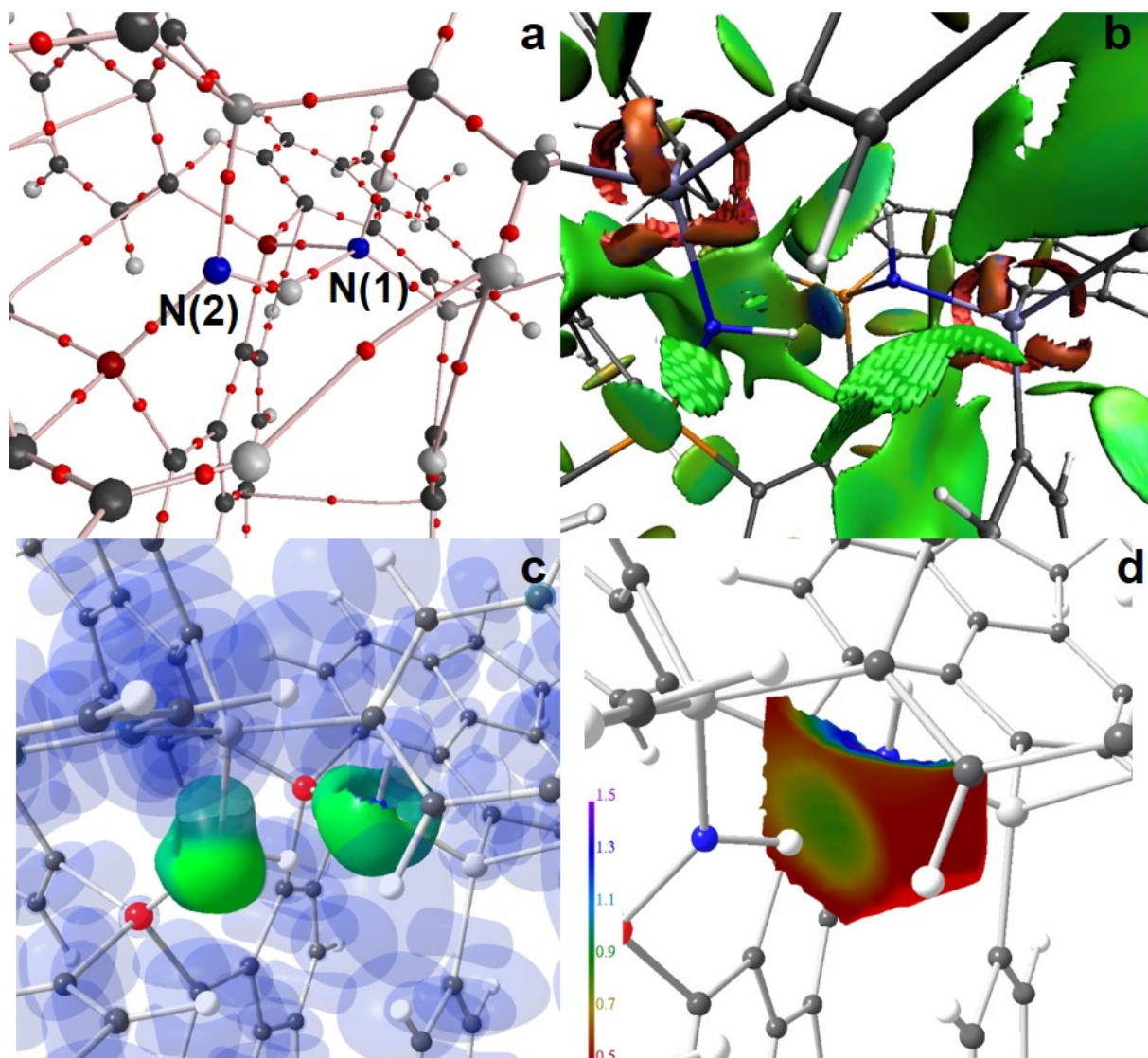


**Figure S19.** RSBI analysis of **6a** (a) AIM bond paths motif, (b) NCI *iso*-surface at  $s(\mathbf{r}) = 0.5$ , (c) ELI-D localization domain representation at *iso*-value of 1.35, (d) ELI-D distribution mapped on the N–N ELI-D bonding basin. Magnification of the active site. Atom colors: P (red or orange), Si (light gray or light blue), N (blue), C (dark grey).